JOURNAL OF SOLID STATE CHEMISTRY 2, 78–93 (1970)

Mixed Oxides of Titanium and Niobium: Defects in Quenched Samples

J. G. ALLPRESS

Commonwealth Scientific and Industrial Research Organization,
Division of Tribophysics, University of Melbourne, Victoria, Australia

Received November 17, 1969

Samples of mixed oxides having the compositions $TiO_2.26Nb_2O_5$ and $TiO_2.7Nb_2O_5$ have been quenched from temperatures near the liquidus, in order to freeze in high concentrations of defects. The structure of the quenched materials has been investigated by electron microscopy. Lattice images of suitably oriented fragments contain sufficient information to enable detailed structural models of the defects within them to be derived. These models indicate that the observed defects, which include Wadsley intergrowth defects and several different kinds of displacements of shear planes, are accommodated coherently and without gross misfit of the components of the structure.

I. Introduction

The concept of nonstoichiometry, as applied to inorganic materials prepared at high temperatures, has required several revisions following the application of single crystal X-ray techniques, and more recently, electron microscopy. A comparison of two reviews on this subject by Wadsley (*1*, *2*), spaced about a decade apart, serves to indicate the substantial developments which were made in this field up to 1964. Further major contributions, particularly by Wadsley and his co-workers since that time have greatly increased our understanding of the role of crystallographic shear and intergrowth in binary oxides containing niobium as a major constituent (*3*). This particular family of oxides (and oxide fluorides) is remarkable for the number of closely related structures which are obtained, and for the way in which these structures can mix, or intergrow, in specific ways, at the unit cell level, to produce intermediate compositions, and sometimes, new ordered phases.

The application of electron microscopy and diffraction (*4–8*) to these materials has led to a much more detailed appraisal of their structures, and the defects which may be found in them. The majority of the defects are produced by the insertion, in a more or less random manner, of very thin planar slabs of related structures in the parent phase. These "Wadsley intergrowth defects"[1] alter the average composition of the crystal very slightly, and unless their concentration is considerable, their presence cannot be detected by conventional X-ray methods.

This paper describes some electron microscope observations of samples of two compositions in the Nb_2O_5–TiO_2 system, which were prepared by quenching from temperatures in the neighbourhood of their melting points. This treatment introduces a high concentration of planar Wadsley intergrowth defects, and in addition, large numbers of more complex defects which have not been described previously.

2. Experimental

2.1. Preparation of Samples

Specimens were prepared from the component oxides in the proportions $TiO_2 \cdot 26Nb_2O_5$ and $TiO_2 \cdot 7Nb_2O_5$. These compositions were chosen because annealed specimens were shown previously to exhibit Wadsley intergrowth of several different structures (*7*). The former was melted in air (ca. 1800°K) on a platinum disk using an induction heater, and cooled rapidly by switching off the r.f. power. The latter was a sample provided by Dr. A. D. Wadsley and had been prepared during an earlier X-ray study (*9*) by sintering the component oxides in air at 1700 °K for 16 hr and quenching the product.

2.2. Electron Microscope Examination

The samples were finely ground and small portions of the powder were collected on carbon-

[1] This name was suggested by Dr. Sten Andersson, at the conference on "The Chemistry of Extended Defects in Non-metallic Solids," held at Scottsdale, Arizona, in April 1969.

coated copper grids and examined in a Philips EM200 electron microscope operated at 100 kV. The microscope was fitted with a cooling device to reduce contamination, and a double-tilting specimen holder. Both the materials studied had one short axis (*b*) of about 3.8 Å, and most of the observations were made on fragments which were oriented with this axis approximately parallel to the electron beam. Most of the images were recorded at orientations where only one set of systematic reflexions was operating—under these conditions a single set of fringes is obtained, and the contrast is usually high. Much more detailed information is obtained from fragments which have their *b* axes exactly parallel to the electron beam, and a large number of *h*0*l* reflexions are operating (*8*). However, the fragments diffract very strongly at this orientation, and contrast is reduced; hence it is successful only in rare cases where the crystals are very thin. Several examples of these two-dimensional images are included in this paper.

3. Results and Interpretation

Electron diffraction patterns and lattice image micrographs of the pure phases in the Nb_2O_5–TiO_2 system have been presented in an earlier publication (*7*). Idealized models of some of the phases which are important for the discussion of the present results are shown in Fig. 1. The structures all contain blocks of corner-shared metal–oxygen octahedra and they differ only in the size of these blocks and the way in which they are joined together. These joints, or *crystallographic shear planes*, are regions of higher-than-average atomic density, where octahedra share edges, and they may also contain metal ions in tetrahedral coordination (black dots marked *O* in Fig. 1.) The shear planes appear as dark lines in electron micrographs of suitably oriented crystals (*4*), and there is also evidence (*8*) that the tetrahedral sites in the shear planes can be correlated directly with dark spots in two-dimensional images.

The orientations of the diffraction patterns, micrographs and structural drawings in this paper have been adjusted so that they are all consistent with respect to each other. In all cases lines of metal atoms within the blocks of octahedra lie parallel to the edges of the pages. This is clearly seen in Fig. 1a.

3.1. Disordered Wadsley Intergrowth

By far the most common type of defects in quenched materials of both compositions were Wadsley intergrowth defects. They also occur in annealed samples, and have been discussed previously (*7*), but frequently the degree of disorder in individual fragments from the quenched samples was very high by comparison with annealed material.

3.1.1. $TiO_2 \cdot 26Nb_2O_5$. The electron diffraction pattern (*h*0*l* reciprocal lattice section) from a quenched fragment of this composition is shown in Fig. 2a. The streaking of the Bragg reflexions in the

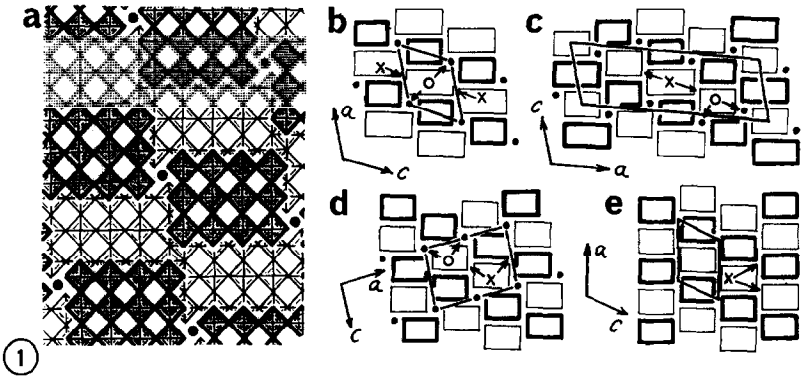

FIG. 1. Idealized models of the structures referred to in this paper.

(a) H–Nb_2O_5, represented as idealized octahedra occurring in blocks, 4 wide × 3 long at one level (heavily outlined), and 5 wide × 3 long at a level half a unit cell down the *b* axis (lightly outlined). Adjacent 4 × 3 and 5 × 3 blocks are joined by sharing edges. The black dots are metal atoms in tetrahedral coordination.

(b) H–Nb_2O_5, a simpler representation in which each block of octahedra is drawn as a rectangle. The unit cell is outlined, and some of the junctions between blocks are labelled—*O*, where blocks are separated by a metal atom in tetrahedral coordination (black dot), and *X*, where blocks are joined by sharing octahedral edges.

(c) $TiNb_{52}O_{132}$, an ordered intergrowth of H–Nb_2O_5 and $TiNb_{24}O_{62}$.

(d) $TiNb_{24}O_{62}$.

(e) $Ti_2Nb_{10}O_{29}$.

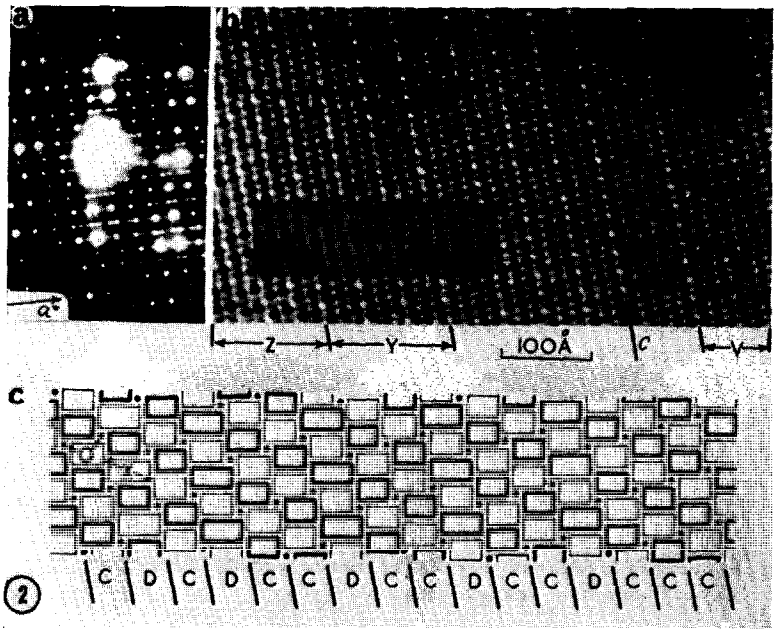

FIG. 2. (a) *h0l* electron diffraction pattern from a quenched fragment of TiO_2–$26Nb_2O_5$.

(b) Two-dimensional lattice image from the same fragment. The regions labelled *V*, *Y* and *Z*, are microdomains of $TiNb_{24}O_{62}$, $TiNb_{38}O_{97}$, and $TiNb_{52}O_{132}$, respectively.

(c) Idealized model of the rectangular area outlined in (b), showing the arrangement of rows or slabs of the component structures $TiNb_{24}O_{62}$ (labelled *C*) and H-Nb_2O_5 (labelled *D*). The inset to (b) shows the arrangement of *O* and *X* positions, taken from the model in (c), and reproduced on the same scale as the lattice image.

direction parallel to a^* is a consequence of disorder in the arrangement of shear planes lying parallel to *c* in the fragment. The detailed nature of the disorder can be established by examining the corresponding two-dimensional lattice image of the fragment; part of which is reproduced in Fig. 2b.

It has been shown (*8*) that a consistent interpretation of images of this type is possible if the dark spots are correlated with the sites of tetrahedrally coordinated metal atoms, or "*O* positions" (Fig. 1). Fig. 2c is an idealized model of the enclosed area in Fig. 2b, derived by making this correlation and by assuming a constant octahedral edge length of 2.89 Å (*5*). It consists of slabs or rows of the two parent structures (Fig. 1) $TiNb_{24}O_{62}$ (labelled *C*), and H–Nb_2O_5 (labelled *D*). It is evident that the arrangement of tetrahedral sites (black dots) is similar to that of the dark spots in the lattice image, and the correspondence is shown clearly in the model inserted in Fig. 2b, which was derived from Fig. 2c by reproducing the black dots on the same scale as the image. The points marked *X* in the inset correspond to *X positions* in the model (see also Fig. 1), where blocks of octahedra are joined directly by sharing edges and differ from the *O positions* where the blocks are separated by metal atoms in tetrahedral co-ordination. The *X* positions appear to correspond to areas of lighter contrast in the lattice image. The detailed examination of images of this type enables microdomains of various compositions to be identified; for example the areas marked *V*, *Y*, and *Z* in Fig. 2b, correspond to the compositions $TiNb_{24}O_{62}$, $TiNb_{38}O_{97}$, and $TiNb_{52}O_{132}$, respectively.

3.1.2. *$TiO_2 \cdot 7Nb_2O_5$*. Fragments of this composition were shown previously (*7*) to exhibit intergrowth of two related structures with compositions $M_{13}O_{33}$ and $M_{12}O_{29}$ (M = metal). A third component was observed in quenched samples, and is evident in one-dimensional lattice images such as Fig. 3a. In addition to a set of wide and narrow black fringes, characteristic of the shear planes in $M_{13}O_{33}$ and $M_{12}O_{29}$, respectively (*7*), there are four wide white fringes, labelled *N*. A likely interpretation of these wider fringes is that they are due to the intergrowth of a row of blocks of octahedra 4 long × 4 wide, in contrast to the $M_{13}O_{33}$ and $M_{12}O_{29}$ structures which contain only 4 × 3 blocks. The model in Fig. 3b indicates how these rows are accommodated. The parent structure, containing 4 × 4 blocks of this type (Fig. 3c) has the composition M_2O_5; the *N* form of Nb_2O_5 has this structure (*10*).

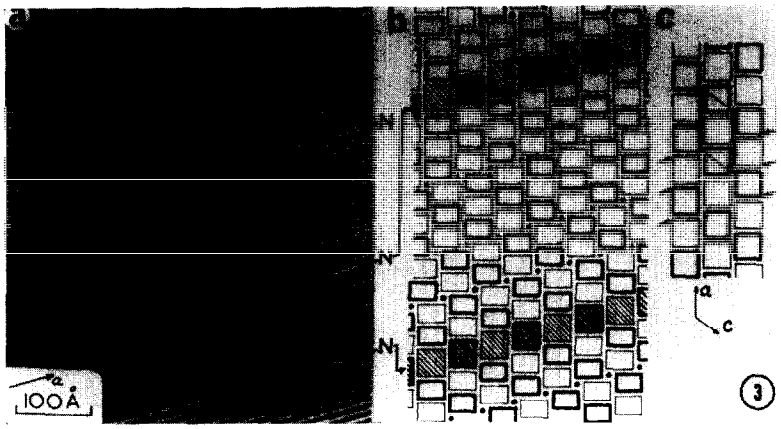

FIG. 3. (a) One-dimensional lattice image from a quenched fragment of $TiO_2 \cdot 7Nb_2O_5$, showing the shear planes as dark lines, and several wide white fringes, labelled *N*.

(b) Idealized model of the enclosed area, in which the heavy black lines in (a) are identified with shear planes containing *O* positions, characteristic of the $M_{13}O_{33}$ structure, and lighter black lines with shear planes containing *X* positions, characteristic of the $M_{12}O_{29}$ structure. The wide white fringes in (a) are interpreted as rows of blocks of octahedra, 4 long × 4 wide (hatched) intergrown amongst the rows of 4 × 3 blocks.

(c) Idealized structure of $N\text{-}Nb_2O_5$, containing only 4 × 4 blocks, arranged in a similar way to the hatched blocks in (b).

The distance between the shear planes marked by arrows on Fig. 3c, calculated from the unit cell dimensions of $N\text{-}Nb_2O_5$[2] is 13.7 Å, in satisfactory agreement with the observed spacing measured on the micrograph by means of a microdensitometer, of 13 ± 1 Å.

3.2. Displacements Parallel to *b*

3.2.1. *$TiO_2 \cdot 26Nb_2O_5$*. The observations discussed in Section 3.1 have been satisfactorily interpreted in terms of the intergrowth of slabs of material which are planar and parallel to the short *b* axis of the structures. However, quenched fragments contained additional defects; examples of the most frequent of these are shown in Fig. 4a. This lattice image was obtained from a crystal tilted so that only reflexions of the type *h*00 were operating, and it shows the shear planes as dark lines lying parallel to *c*, and separated by 15 Å across a *C* row of $TiNb_{24}O_{62}$ and 17 Å across a *D* row of $H\text{-}Nb_2O_5$ (*C* and *D* as in Fig. 2). The majority of the shear planes are straight, but several of them deviate in the areas outlined. This has the effect of changing a *C* row to *D* and vice versa.

The simplest possible geometry for a displacement defect of this type is sketched diagrammatically in Fig. 4b, which is intended to represent the arrangement of shear planes parallel to *c* in a thin slab of the structure whose projection is outlined by a rectangle in Fig. 4a. The difference in width of the *C* and *D* rows is exaggerated in order to show the proposed structure more clearly. The displacement is drawn as a step, linear and parallel to *b*, in the shear plane marked with an arrow. Its image should therefore be sharp when viewed directly down the *b* axis. The micrograph in Fig. 4a was obtained from a fragment tilted slightly from this orientation, hence the image of the displacement would be expected to be slightly extended in the direction of tilt, i.e., in the same direction as the shear planes. This is the probable reason for the fact that the transition from a *C* row to a *D* row in the vicinity of the defects in Fig. 4a is not sharply defined.

Possible idealized structures for these defects can be derived from the information contained in the micrographs by building models of the surrounding area, using the criteria developed previously (*7*), and investigating their appearance in the vicinity of the displacement. The area outlined by the rectangle in Fig. 4a was treated in this way, and the idealized model shown in Fig. 4c was obtained. The displacement occurs in the shear plane marked by an arrow, and the *D* row affected by it is hatched. The model shows that the defect can be accommodated without any gross misfit of the structural components and the proposed structure involves only a small local alteration in the arrangement of blocks of octahedra. The hatched *D* row in Fig. 4c is continuous and overlaps in the vicinity of the defect, and the neighbouring *C* row is discontinuous. The reverse situation, in

[2] $a = 28.51$ Å, $b = 3.830$ Å, $c = 17.48$ Å, $\beta = 124.8°$. The value of β differs from that quoted by Andersson in his paper (*10*), the latter being a transcription error (S. Andersson, personal communication.)

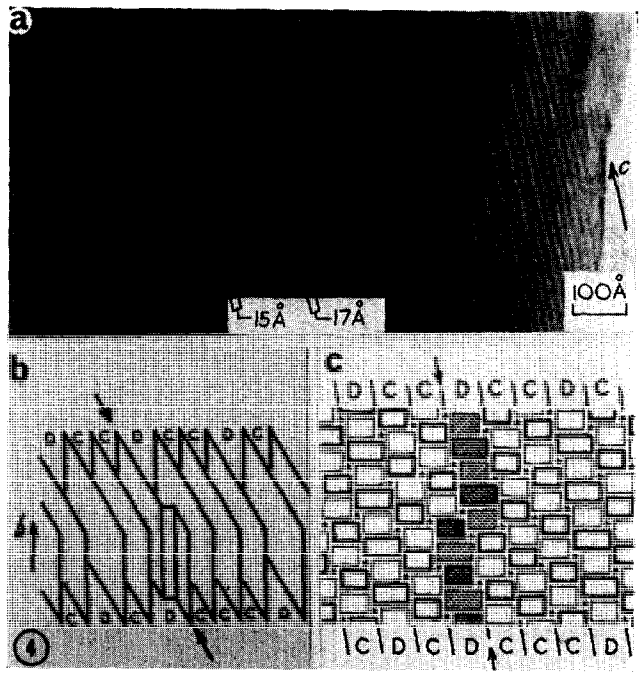

FIG. 4. (a) Lattice image of a quenched fragment of $TiO_2 \cdot 26Nb_2O_5$, containing several displacement defects parallel to *b* in the areas outlined. The dark lines are the shear planes, and their separations are either 15 Å across a *C* row of $TiNb_{24}O_{62}$, or 17 Å across a *D* row of H–Nb_2O_5.

(b) Sketch showing the arrangement of shear planes in the neighbourhood of the displacement parallel to *b* outlined by a rectangle in (a). The difference in spacing of *C* and *D* rows is exaggerated to show clearly the detail of the displacement in the shear plane marked by an arrow.

(c) Idealized model of the area outlined by a rectangle in (a). The component blocks of the *D* row which is affected by the displacement are hatched. The shear plane containing the displacement is marked by an arrow.

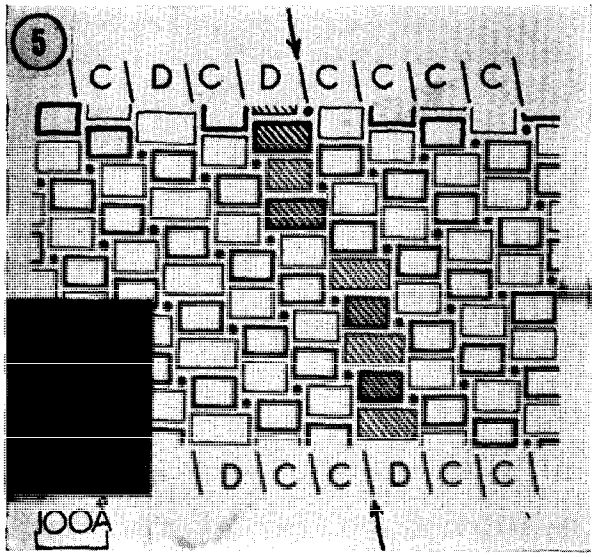

FIG. 5. Idealized model of a displacement parallel to *b* whose direction is opposite to that shown in Fig. 4. The *D* row affected by the displacement is hatched. The inset is part of a micrograph of a fragment of $TiO_2 \cdot 26Nb_2O_5$, showing the lattice image from such a displacement.

which the *D* row is discontinuous and the *C* row overlaps in the vicinity of the defect (Fig. 5) applies when the direction of the displacement is opposite to that illustrated in Fig. 4. Displacements in this direction, exemplified by the lattice image reproduced in the inset to Fig. 5, were rarely observed.

The increased detail found in two-dimensional images of fragments containing displacement defects provides confirmation of the proposed structures, but indicated an additional unsuspected complexity. The image in Fig. 6a (which is a magnified portion of Fig. 12b) shows a single *D* row (marked) containing a number of displacements (*P*, *Q*, *S*) in a matrix of surrounding *C* rows. The contrast in the vicinity of the defect labelled *S* differs slightly from that near those labelled *P*; the former has an additional dark dot. The defect *Q* is a multiple displacement, where the *D* row shifts two rows sideways instead of one. An idealized block model of the area outlined in Fig. 6a is shown in Fig. 7a. This model was derived by correlating the dark spots in the image with sites of tetrahedral coordination (*O* positions) in the structure, in the

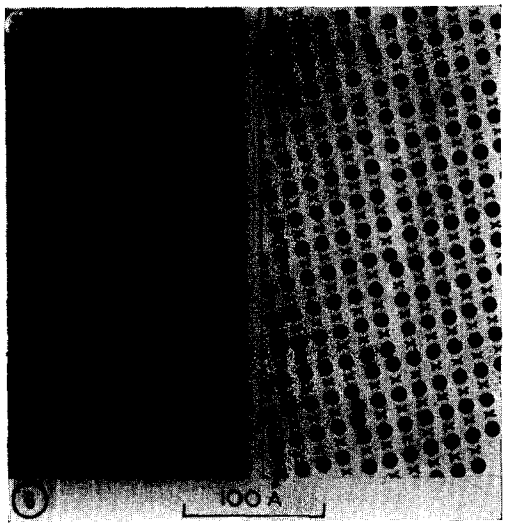

FIG. 6. (a) Two-dimensional image from a quenched fragment of $TiO_2 \cdot 26Nb_2O_5$ showing several displacements (P, Q, S) along a D row (marked) in a matrix of surrounding C rows.

(b) The arrangement of O positions (black dots) and X positions (marked X) taken from an idealized model of the area in Fig. 6(a) and reproduced at the same magnification of the micrograph. The arrangement includes the effects of a step in the displacement labelled S in Fig. 6(a).

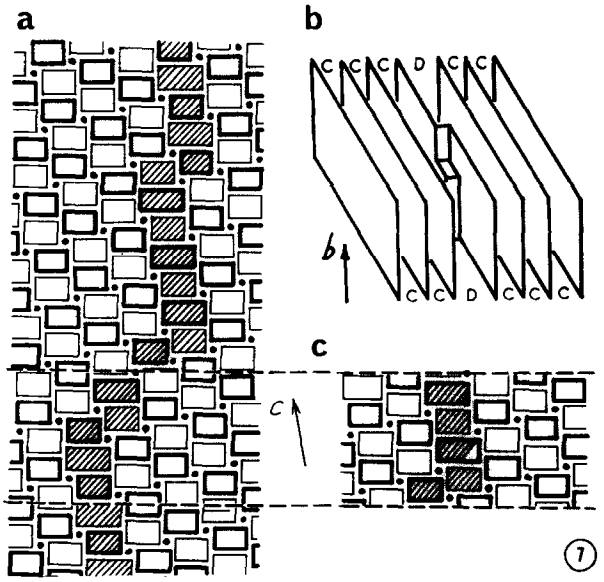

FIG. 7. (a) Idealized model of the area outlined in Fig. 6(a). The model does not adequately account for the contrast in the vicinity of S in Fig. 6 (a).

(b) Sketch of a displacement parallel to b containing a step, postulated in order to explain the contrast at S in Fig. 6(a).

(c) Idealized model of the area in the vicinity of S in Fig. 6(a), but *below* the step. When superimposed on the area of Fig. 7(a) between the dotted lines, the observed contrast in Fig. 6(a) is reproduced.

same way as for Fig. 2. In the vicinity of the defect P, the model corresponds exactly with the one proposed earlier (Fig. 4) using information from a one-dimensional image. This confirms the earlier assumption that the displacement defect is linear and parallel to b because it gives sharp contrast in the two-dimensional image where the fragment is oriented with its b axis parallel to the electron beam. The model also satisfactorily accounts for the structure of the multiple displacement at Q. However, the additional dark spot in the image of the defect labelled S is *not* reproduced in Fig. 7a. A variety of structures were considered in an attempt to reproduce this contrast, and only one of these fitted the observed image. It became necessary to suggest that the displacements need not be strictly linear in the b direction, but may contain a *step*, and that the contrast from the resulting compound defect is the superposition of that expected from the structures above and below the step. A diagrammatic sketch of a step on a displacement defect is shown in Fig. 7b (compare Fig. 4b). The defect labelled S in Fig. 6a is considered to have the structure modelled in Fig. 7a (between the dotted lines) *above* the step, and the structure modelled in Fig. 7c *below* the step. The two structures are similar except that in Fig. 7c, the displacement defect is shifted along the shear plane. When the two structures are superimposed, the distribution of tetrahedral sites (O positions) corresponds to the distribution of dark spots in Fig. 6a. This is clearly seen in Fig. 6b, which shows the arrangement of O positions (black dots) and X positions derived from an idealized model of the whole area of Fig. 6a. The agreement with the observed contrast throughout the figure is satisfactory.

The detailed structure of the fragment in the vicinity of the step is difficult to describe without the aid of a three-dimensional model. However, the construction of such a model has shown that the structures above and below the step, illustrated in plan in Fig. 7a and c, fit together coherently when placed one on top of the other, and do not involve any misfit of the structural components. Some further discussion of the detailed structure appears in Section 3.4, where displacements perpendicular to b are described.

3.2.2. $TiO_2 \cdot 7Nb_2O_5$. Displacements parallel to b are evident in the micrographs reproduced in Fig. 8. Fig. 8a is a one-dimensional image and shows that the displacements can occur in two directions, in the rows marked Y and Z respectively. Idealized

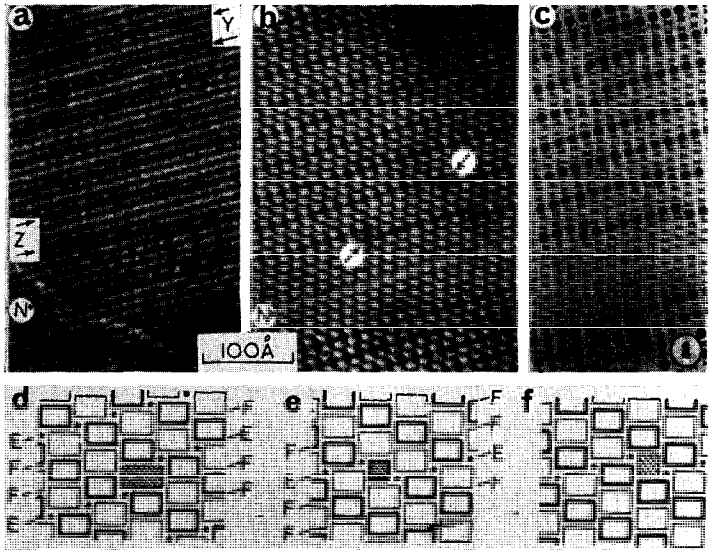

FIG. 8. (a) One-dimensional image from a quenched fragment of $TiO_2 \cdot 7Nb_2O_5$, showing displacements in two directions, in the planes labelled *Y* and *Z*, respectively. A row of 4 × 4 blocks, labelled *N*, is also present in the area.

(b) Two-dimensional image of the same area. The arrows mark displacements which contain a step.

(c) Arrangement of *O* and *X* positions, derived from an idealized model of most of the area of (b), and including the effects of a step in each of the displacements marked by arrows in (b).

(d) Idealized model of a displacement of the type seen in the planes marked *Y* in Fig. 8(a). The hatched block is 5 octahedra × 3 in size, the remainder are 4 × 3. The shear planes labelled *E* contain *O* positions, those labelled *F* contain *X* positions.

(e) Idealized model of a displacement of the type seen in the planes marked Z in Fig, 8(a). The hatched block is 3 octahedra × 3 in size.

(f) This model is identical to (e) apart from a shift in the displacement. The superposition of (e) and (f) is necessary in order to explain the contrast around the defects marked by arrows in (b), which are assumed to contain a step.

models of these displacements may be derived by the method indicated in Section 3.2.1, and are shown in Fig. 8d and e. General confirmation of these models is obtained by comparison with the detailed two-dimensional image of the same area, shown in Fig. 8b, but in this case also, it is necessary to postulate the presence of a step in the displacement defects marked by arrows, in order to explain the observed contrast. The structures above and below the step are shown in Figs. 8e and f. They differ only in the position of the displacement defect, which is shifted along the shear plane by one block of octahedra in Fig. 8f. The contrast in Fig. 8b is satisfactorily reproduced in Fig. 8c which shows the *O* and *X* positions taken from an idealized model of this region of the crystal, and includes the effects of steps in the displacements marked by arrows. In addition, the intergrowth of a row of 4 × 4 blocks (see Section 3.1.2) marked *N* is accounted for in the model.

The effect of the presence of a displacement defect in $TiO_2 \cdot 7Nb_2O_5$ is to introduce a block of octahedra that differs in size from the surrounding 4 × 3 blocks (Fig. 8d and e). The fault block is either 5 × 3 or 3 × 3 depending upon the direction of the displacement. At the same time, the shear planes affected by the displacement are changed. A plane containing metal atoms in tetrahedral coordination (*O* positions, labelled *E* in Fig. 8d and e) is converted to one in which blocks are joined by sharing octahedral edges (*X* positions, labelled *F* in Fig. 8d and e) as it passes the defect.

3.3. Displacements Perpendicular to *b*

A very few examples of defects that produce a displacement of a shear plane perpendicular rather than parallel to *b* were observed in quenched $TiO_2 \cdot 26Nb_2O_5$. This situation, which is closely related to the case of a step on a parallel displacement (see Fig. 7) is represented schematically in Fig. 9a, and the two-dimensional lattice image reproduced in Fig. 10 contains evidence for the presence of defects of this type. This micrograph was taken from a different area of the same fragment as was imaged in Fig. 2, and in spite of its relatively poor quality, similarities with Fig. 2 are easily recognized. The contrast in the area *V* is characteristic of the composition $TiNb_{24}O_{62}$, consisting entirely of *C*

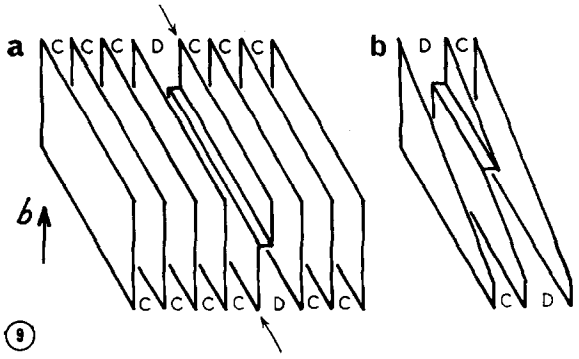

FIG. 9. (a) Sketch of a displacement perpendicular to *b*, in the shear plane marked by an arrow.

(b) Sketch of a similar displacement in a wedge-shaped crystal, showing how the displacement may "run out" of the crystal at some distance from its edge.

rows, except for the defect marked by an arrow. Most of the area *Z* shows contrast typical of the row sequence *–C–D–C–D–*, characteristic of $TiNb_{52}O_{132}$. However, the contrast along the rows marked by arrows in Fig. 10 differs from that seen in Fig. 2.

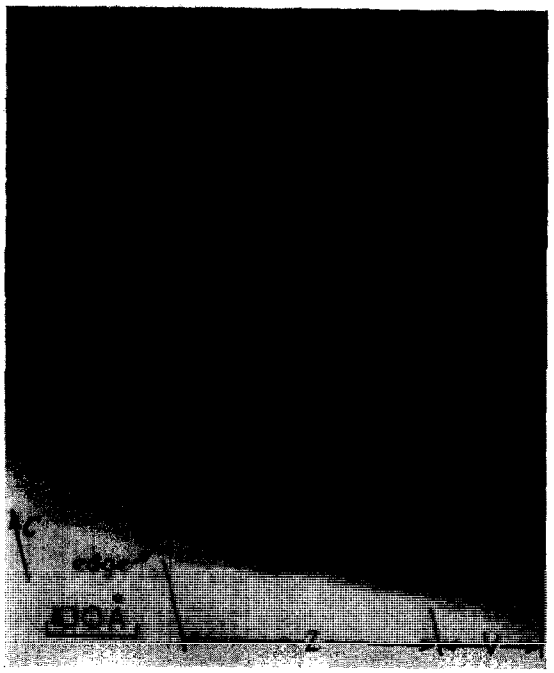

FIG. 10. Two-dimensional lattice image from $TiO_2 \cdot 26Nb_2O_5$, showing overlapping contrast in the rows marked by arrows, due to the presence of displacements perpendicular to *b*. The contrast returns to normal near the edge of the fragment because in this region, the displacement defect has "run out" of the fragment as shown schematically in Fig. 9(b). The regions marked *V* and *Z* correspond to micro-domains of $TiNb_{24}O_{62}$ and $TiNb_{52}O_{132}$, respectively.

The lines of dark spots which run approximately perpendicular to *c* *overlap* along these rows, and the overlap does not extend to the edge of the crystal. The overlapping contrast is most probably due to the presence of displacements perpendicular to *b*, which run out of the fragment at some distance from its edge, where its thickness is decreasing, as shown schematically in Fig. 9b.

The detailed models in Fig. 11a, b and c are intended to illustrate the proposed structure in the vicinity of a displacement perpendicular to *b*. Fig. 11a and b are plan views of a structure consisting of a single *D* row intergrown in a matrix of *C* rows. In Fig. 11b, the *D* row is shifted with respect to its position in Fig. 11a, and the two plans represent the structure above and below the displacement, respectively. Fig. 11c is the section *A–A* through the structure, and indicates that the sections above and below the displacement fit together coherently; this conclusion was confirmed by making a three-dimensional model of the defect.

It is possible to explain the overlapping contrast in the lattice image on the basis of this structural model, if it is assumed that the image in the vicinity of the defect is simply the superposition of the images expected from the structures above and below the defect. Fig. 11d and e show the arrangement of *O* and *X* positions in a crystal containing a *D* row in a matrix of *C* rows, analogous to the structures shown in Fig. 11a and b. These diagrams represent the contrast expected from the structures above and below a displacement perpendicular to *b*, and they differ only in the position of the *D* row. When these diagrams are superimposed, Fig. 11f is obtained, which contains overlapping contrast similar to that seen in the rows marked by arrows in Fig. 10.

3.4. Arrays of Defects

3.4.1. $TiO_2 \cdot 26Nb_2O_5$. In many fragments, the concentration of displacement defects was very high and they tended to form lines which lay at an angle to the shear planes. In the one-dimensional image in Fig. 12a, the individual displacements have the same appearance as those illustrated in Fig. 4a, and they are arranged in randomly spaced lines, marked by arrows. Between these lines, the image consists of a regular sequence of 15 and 17Å fringes parallel to *c*, characteristic of a well-ordered Wadsley intergrowth of *C* and *D* rows, with the composition $TiNb_{52}O_{132}$.

The two-dimensional image in Fig. 12b contains sufficient detail to permit a precise comparison of a proposed structure and the lattice image. The

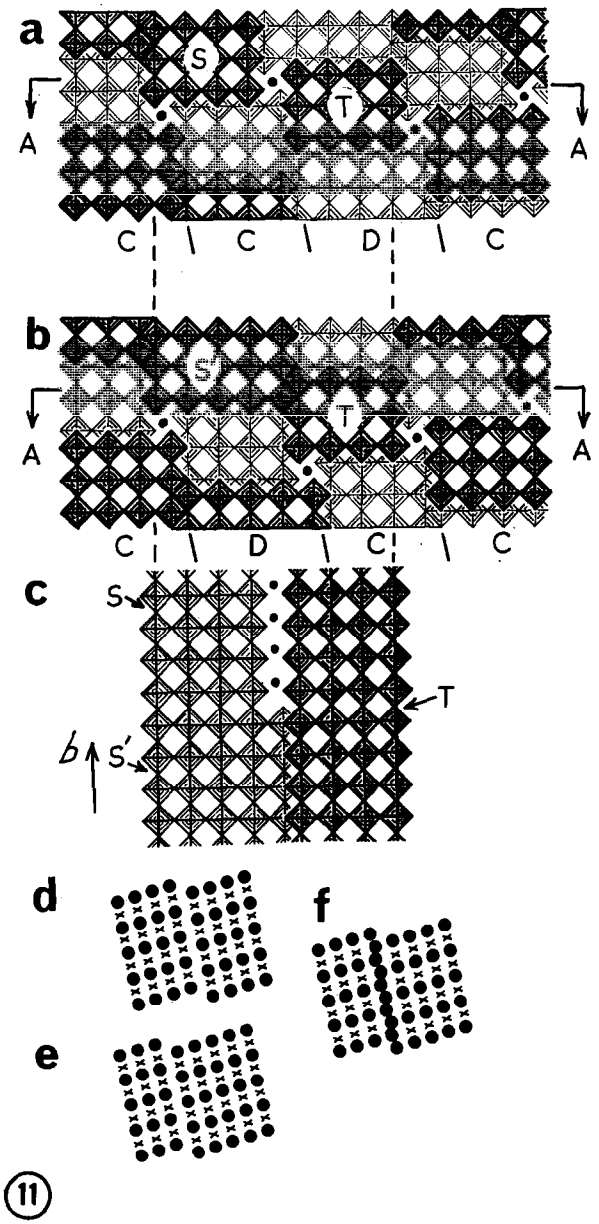

FIG. 11. (a–c) Detailed idealized model of a displacement perpendicular to *b*. a and b are plan views of the structure above and below the displacement respectively, and *c* is the section *A–A* through the structure. The defect occurs when the block labelled S (4 × 3) changes to S′ (5 × 3). Above the defect, *S* and *T* are separated by metal atoms in tetrahedral coordination (black dots); below it, *S′* and *T* are joined by sharing octahedral edges.

(d–f) Derivation of the overlapping contrast due to a displacement perpendicular to *b*. (d) and (e) represent the arrangement of *O* and *X* positions in the structures above and below the defect, respectively, for the case of a single *D* row in a matrix of C rows. The diagram (f) is the superposition of (d) and (e), and shows overlapping contrast similar to that in the rows marked by arrows in Fig. 10.

micrograph indicates that there are regions of well ordered $TiNb_{24}O_{62}$, such as *C*, interrupted by a set of lines of defects which wander across the crystal. In a few places, such as at *D*, these lines are straight and their appearance is typical of the presence of a *D* row of the H–Nb_2O_5 structure. In the regions where the lines deviate, the density of dark spots increases (e.g., *Z*). It is possible to account for the observed contrast in terms of the presence of single or multiple displacements parallel to *b*, some of which contain steps perpendicular to *b*. A detailed analysis of the area outlined in Fig. 12b has been presented earlier (Figs. 6 and 7, Section 3.2.1).

The lines of displacement defects may be much closer together and more regular than is indicated in Fig. 12, and in these circumstances, their presence is manifested in electron diffraction patterns by a shift of most of the weak reflexions. A comparison of the diffraction patterns from annealed and quenched fragments, shown in Fig. 13a and b respectively, illustrates the effect. The positions of the strong reflexions in both patterns are similar, but whereas in Fig. 13a, the reflexions all lie in straight lines parallel to a^*, in Fig. 14b the weak reflexions are shifted alternately to either side of these lines. About ten fragments having this type of diffraction pattern have been found amongst the hundreds which have been studied. Amongst these ten, there is some variation in the extent of the observed shifts of the weak reflexions in the diffraction patterns. Typical one dimensional lattice images of these fragments are shown in Fig. 13c and d. In addition to the set of straight fringes parallel to *c*, corresponding to the shear planes, a second set of diffuse and much less regular fringes traverse the images. In Fig. 13c these fringes lie at an angle of about 24° to the shear planes, and their spacing is about 40 Å; these values correspond reasonably well to those derived from the spacing and orientation of adjacent weak spots in the diffraction pattern, such as those encircled in Fig. 13b. In Fig. 13d the separation of diffuse fringes varies considerably and their concentration drops to zero on the right hand side of the micrograph. At first sight, they might well be described as Moiré fringes arising from separate overlapping crystals. However, the diffraction pattern (Fig. 13b) is unlike that expected from overlapping crystals. In addition, the contrast in the right hand portion of Fig. 13d is typical of that due to the intergrowth of several 17 Å *D* rows containing isolated displacements parallel to *b*, and it seems most likely that the changing appearance of the image as one moves to the left is simply due to an increase in the number of

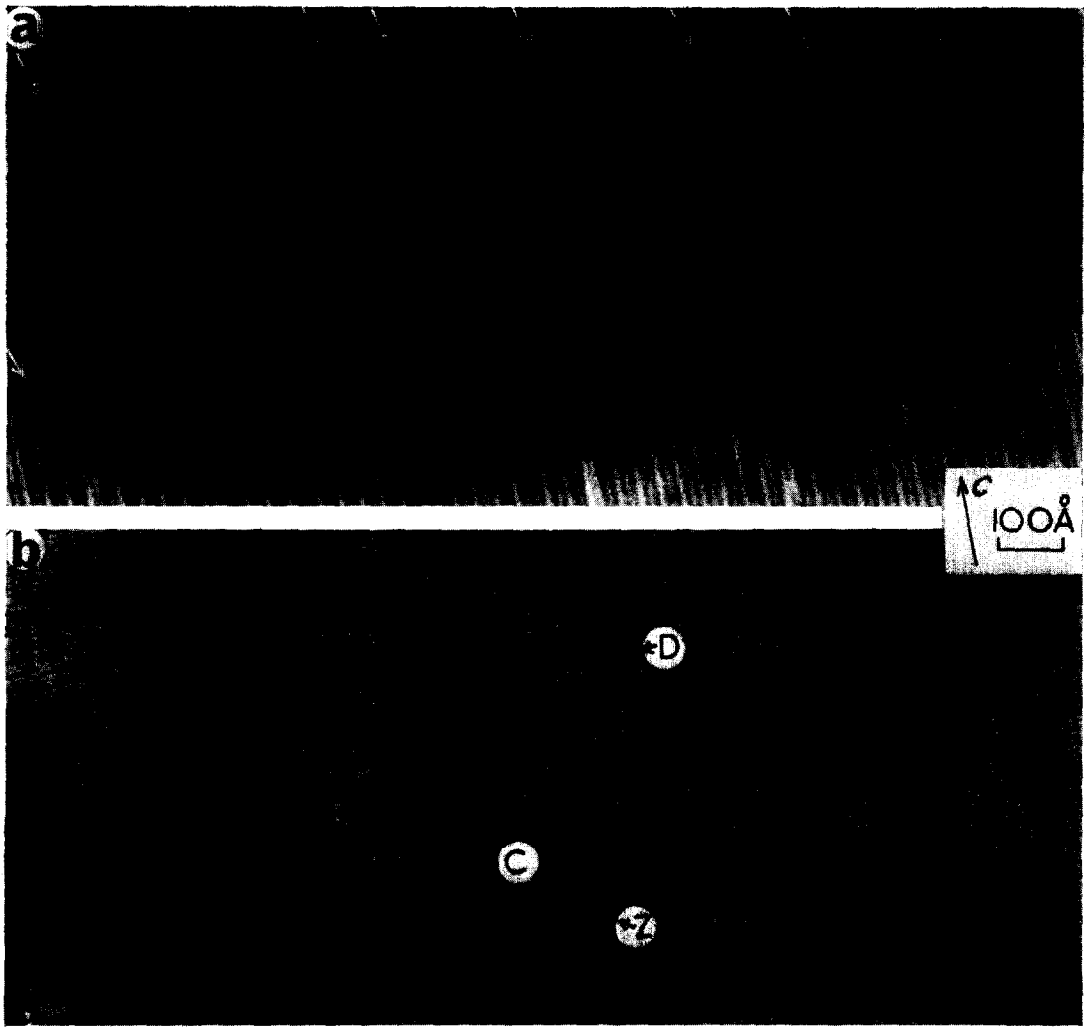

FIG. 12. (a) One-dimensional image of a quenched fragment of $TiO_2 \cdot 26Nb_2O_5$ showing a well-ordered intergrowth of *C* and *D* rows (15 and 17 Å wide, respectively), traversed by a series of lines of displacements parallel to *b*, marked by arrows.
(b) Two-dimensional image from another fragment, consisting largely of $TiNb_{24}O_{62}$ (e.g., the area *C*), traversed by a number of *D* rows (e.g., *D*) each containing many displacement defects, particularly in regions where the concentration of dark spots is high (e.g., at *Z*). The area outlined by the rectangle has been analysed in detail in Figs. 6 and 7.

these displacements along each *D* row. This implies that each of the diffuse fringes corresponds to a *D* row displaced frequently along its length. The total width of 50 shear-plane fringes marked *Y–Y* on Fig. 13d, crossed by 12 diffuse fringes, is 767 Å, which corresponds well with that of 764 Å calculated for 12 *D* rows (each 16.8 Å) plus 38 *C* rows (each 14.8 Å).

A number of attempts have been made to explain both the unusual diffraction patterns and the images in terms of models, but none have yet given a completely satisfactory correspondence with the observations. This is clearly a case where a two-dimensional image of a suitably thin fragment is required and it is hoped that such a fragment will be found eventually.

3.4.2. $TiO_2 \cdot 7Nb_2O_5$. Extensive arrays of the kind just described were not observed in crystals of this composition, possibly because the quenching conditions were rather different for this sample. Several micrographs showing lines of defects are included to show the types of effects which were frequently observed, and also to demonstrate the contrast effects which may be obtained from various orientations of the same fragment.

Fig. 14a is a two-dimensional image of a fragment; part of this image is reproduced in Fig. 8b. Most of the defects which are evident in this image are of the

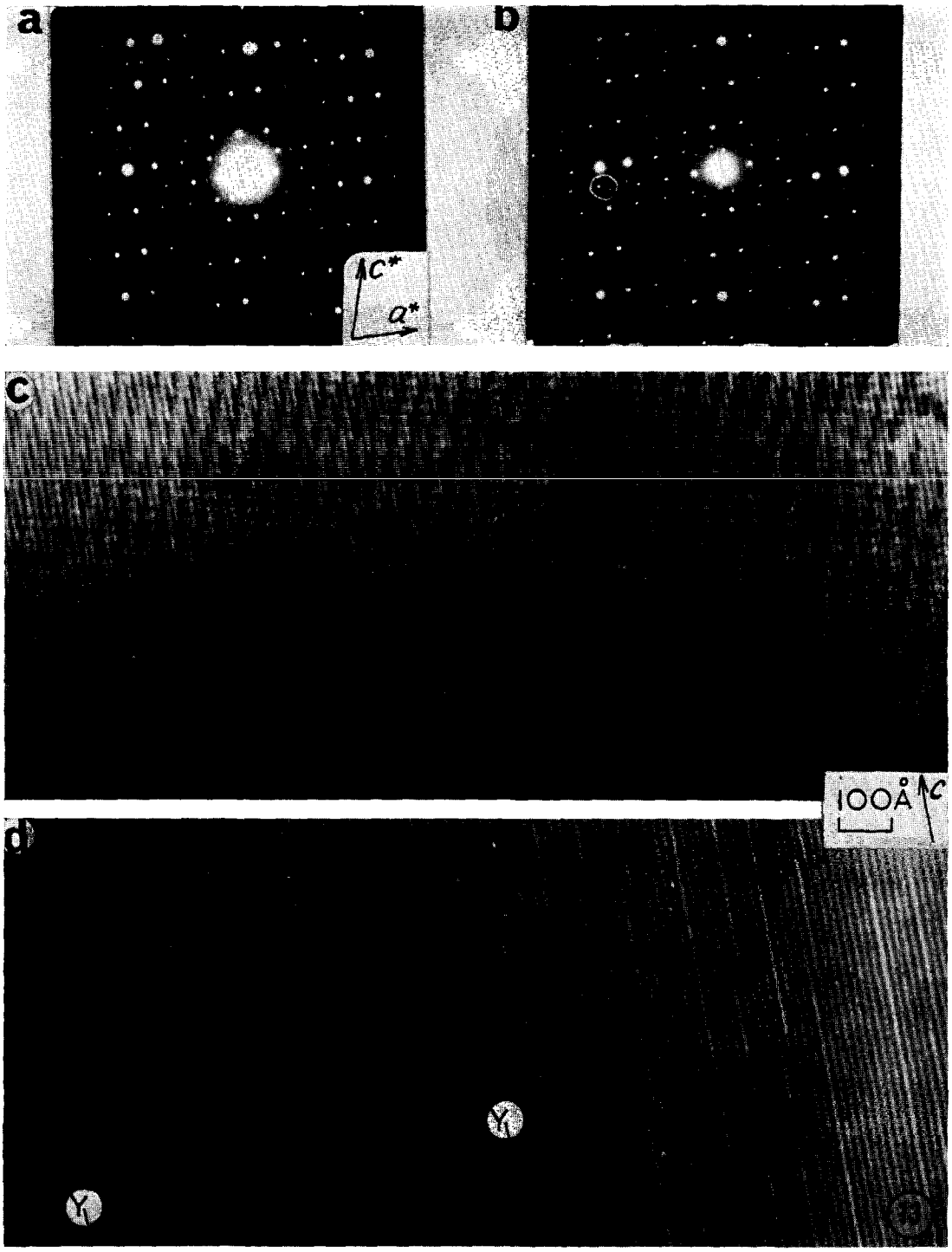

FIG. 13. (a–b) Electron diffraction patterns (*h0l* reciprocal lattice sections) of well annealed and quenched samples of $TiO_2 \cdot 26Nb_2O_5$, respectively. In (b), the weaker reflections are displaced with respect to their regular positions in (a).

(c–d) One-dimensional lattice images of quenched fragments of the above composition, in which concentration of displacement defects is very high. In (c), the fringes parallel to *c*, due to the shear planes, are intersected by a much less regular set of diffuse fringes, about 40 Å apart, due to the lines of parallel displacements. In (d), the 17 Å *D* rows on the right contain relatively few isolated displacements, but their concentration increases across the figure, and they form closely spaced lines similar to those in (c) on the left.

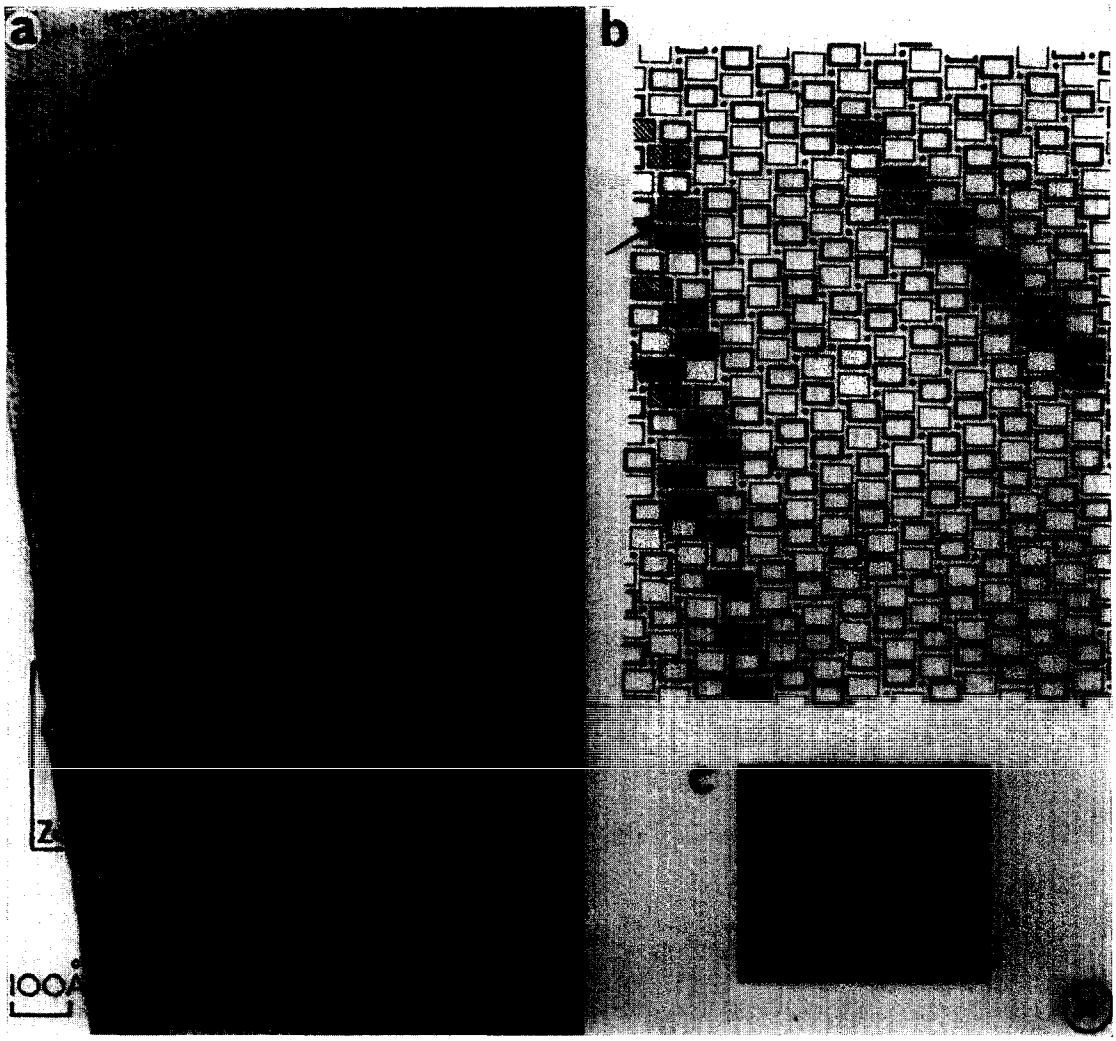

FIG. 14. (a) Two-dimensional lattice image of a quenched fragment of $TiO_2 \cdot 7Nb_2O_5$.
(b) Idealized model of the left hand part of the area enclosed by the rectangle in (a). The hatched blocks are 5 × 3, all others are 4 × 3. A junction between blocks of the type found in M–Nb_2O_5 is marked by an arrow.
(c) Arrangement of *O* and *X* positions, derived from an idealized model of the area outlined in (a).

kind already described in Sections 3.1.2 and 3.2.2. However, the fault running along the edge of the fragment, containing two very heavy black spots marked Z requires additional discussion. A possible model for this fault in the region enclosed by the rectangle is shown in Fig. 14b. It includes junctions between blocks which differ slightly from the *X* positions normally found in materials of this composition. However, junctions of the type marked by an arrow in Fig. 14b are found in the *M* form of Nb_2O_5 (*11*). The origin of the very heavy contrast at *Z* in Fig. 14a is unknown at present—no other instances of this contrast have been observed. In a one-dimensional image of the same area, the contrast at *Z* was completely absent. This is probably the only region in Fig. 14a which cannot be satisfactorily interpreted. Fig. 14c is a model of the enclosed area in Fig. 14a, showing only *O* and *X* positions (*X* includes all junctions which involve octahedral edge-sharing) which reproduces the observed contrast reasonably well.

Fig. 15a–c shows three different images of another fragment, taken at the orientations indicated by the diffraction patterns in Fig. 15e–g respectively. The *h*0*l* diffraction pattern of the same fragment is shown in Fig. 15d. Fig. 15a and c are one-dimensional images, showing the two sets of intersecting shear planes separately. In (b) the

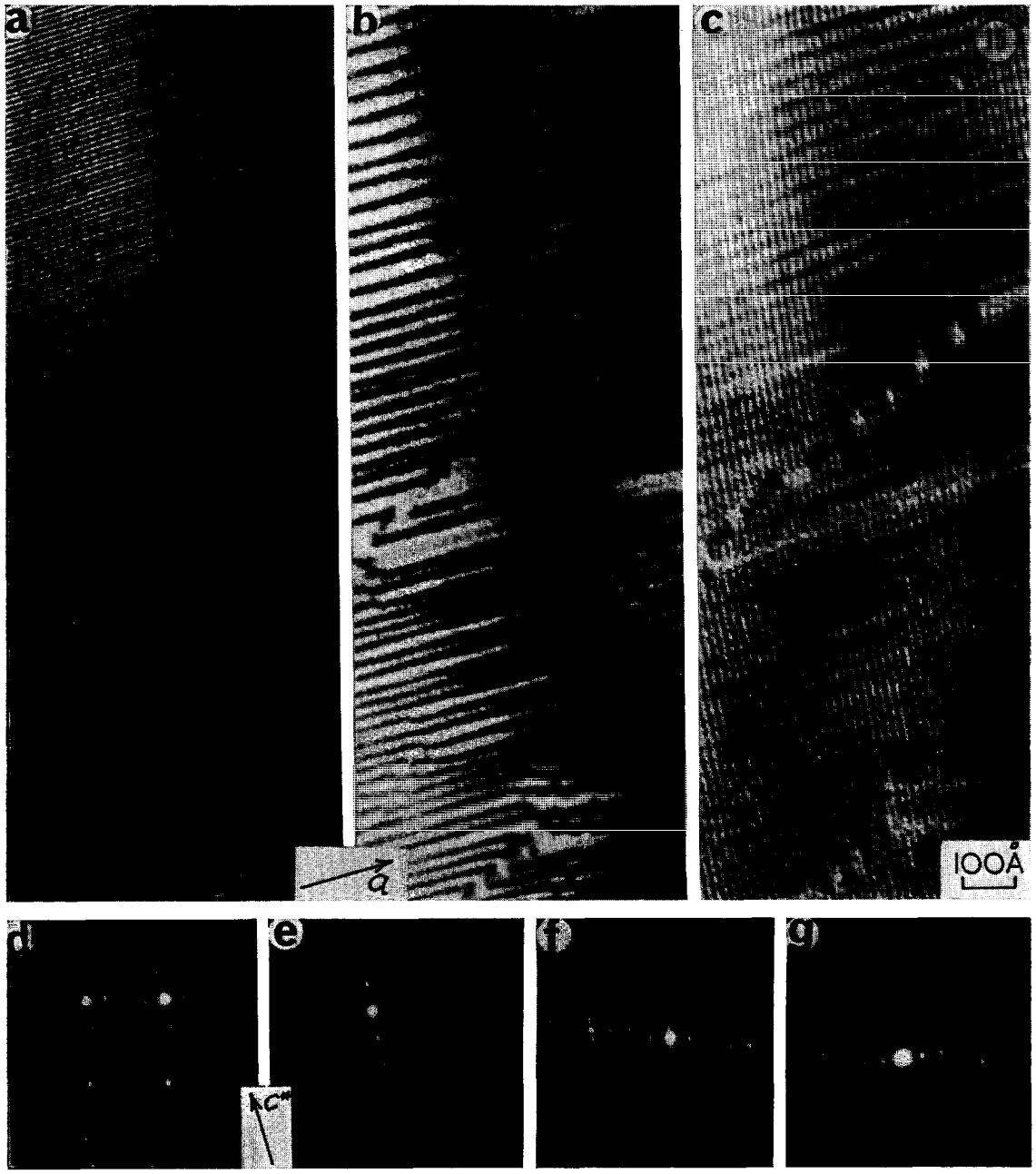

FIG. 15. (a–c) Lattice images of the same area of a quenched fragment of $TiO_2 \cdot 7Nb_2O_5$, showing the contrast effects produced by altering the orientation of the fragment.

(d–g) Electron diffraction patterns of the same fragment. (d) is the *h0l* reciprocal lattice section, and the images (a), (b), and (c) are taken with the fragment oriented to give the patterns (e), (f), and (g), respectively.

fragment is slightly tilted from its position in (c), in order to include a restricted contribution from reflexions parallel to c^*. The shear planes in (c) are only just visible in (b); most of the contrast in (b) is in lines parallel to the shear planes in (a), and the defects in the structure are much more apparent in this image than in either of the other two. The reason for the enhanced contrast is not fully understood, but is certainly related to the fact that the contribution from reflexions parallel to c^* is limited

and the contrast from planes with spacings of less than about 15 Å is suppressed. There is a considerable correlation between the lines in (b) and the wide black lines in (a), which correspond to shear planes containing tetrahedral sites. The contrast in (b) becomes more diffuse in the thicker region of the fragment on the right side of the micrograph because the shear planes parallel to *a* are not exactly perpendicular to the electron beam in this orientation. While it is possible to interpret some areas of these images with reasonable confidence, the complexity of the defect structure evident in the central region of Fig. 15b is such that two-dimensional images would be required in order to derive a convincing model. At first sight it might appear that the lines in Fig. 15b which terminate within the image could be *dislocations*. However, it seems clear from Fig. 15a that this is not the case; the terminations in (b) probably correspond to changes in the sequence of shear planes associated with the passage of a row containing a series of displacements parallel to *b*.

4. Discussion

4.1. Completeness of the Observations

The observations which have been described in Section 3 are representative of a large number of results recorded for many different fragments of these two quenched compounds. In many cases, the arrangement of defects was very complex, and the images which were obtained were not of sufficiently good quality to enable detailed models to be worked out. However, it is reasonably certain that these complex arrangements could always be resolved into some combination of the individual defects which have been discussed in detail in Sections 3.1, 3.2, and 3.3, i.e., Wadsley intergrowth defects, displacements parallel to *b* (with or without steps), and displacements perpendicular to *b*. The main reason for the lack of a complete interpretation of a larger number of observed arrays is simply that in these complex situations, two-dimensional images are almost essential in order to derive models with reasonable certainty. The number of these images which have been recorded to date is very small. It is perhaps worth pointing out that on any particular electron microscope specimen grid, only a small fraction (say 10%) of the fragments are sufficiently thin to justify examination. Of these, perhaps 40% can be tilted into a suitable orientation to obtain a one-dimensional image. Experience suggests that good two-dimensional images are only obtained from very thin fragments, which may constitute only about 5% of the number that give good one-dimensional images. The value of the detailed contrast in two-dimensional images is well demonstrated in the examples given in this paper and it seems clear that the direct correlations which have been made between this contrast and specific features in the structures is justified, even though the theoretical basis for this correlation is at present rather obscure (*8*).

4.2. Stoichiometry of Quenched Samples

It is evident that the composition of any particular fragment will be influenced by the presence of defects of the kind which are revealed in the lattice images. It has already been shown (*5–7*) that Wadsley intergrowth defects are probably the most important source of nonstoichiometry in this family of materials, and this remains true for the quenched samples. The effect of displacement defects on composition is relatively small by comparison, and will be discussed in detail in connection with their diffusion in a subsequent paper (*12*). Reference to the models in Fig. 4c, 5, and 8d and e suggests that the effect of a parallel displacement depends upon its direction. In Fig 4c, the *D* row affected by the displacement (hatched) overlaps itself, and the neighbouring *C* row is discontinuous. Hence, the amount of *D type* structure, of composition Nb_2O_5, is slightly increased by the presence of the defect. Conversely, in Fig. 5, the direction of the displacement is reversed, and the amount of *C type* structure of $TiNb_{24}O_{62}$ is increased. In Fig. 8d, the presence of a 5×3 block of octahedra (hatched) amongst 4×3 blocks will slightly increase the overall oxygen–metal ratio, and in Fig. 8e, the presence of a 3×3 block will have the reverse effect.

It would be dangerous to assume that these are the *only* sources of nonstoichiometry; there may well be a contribution from defects which are not resolved in the electron microscope images presented here. In particular, the concentration of point defects such as vacant lattice sites and interstitial atoms cannot be derived from the present observations. The existence of defects of this kind has frequently been invoked in order to explain nonstoichiometry in Nb_2O_5, and in most cases, the results of thermogravimetric experiments and observations of properties such as electronic conductivity have been interpreted on this basis (*13*). While it is possible in principle to explain *all* the nonstoichiometry quite satisfactorily in terms of intergrowth and displacement defects, this is not in itself a sufficient justification for ignoring the presence of point defects. In support of this, it has been shown that the compound $WNb_{12}O_{33}$ (*14*) (which

has a structure closely related to that of H–Nb_2O_5) has a range of homogeneity from $6Nb_2O_5 \cdot WO_3$ ($MO_{2.54}$) to about $8Nb_2O_5 \cdot WO_3$ ($MO_{2.53}$) and that annealed samples of the latter composition do *not* contain intergrowth or displacement defects (*16*). This point is under current investigation but it is clearly a case where point defects might be a significant source of the nonstoichiometry.

Reported studies of the properties of H–Nb_2O_5 and similar compounds are frequently accompanied by observations of X-ray powder diffraction patterns of the materials used, which indicate a single phase region over the range of compositions studied. This technique is incapable of detecting intergrowth defects, and it is almost inevitable that these defects are responsible for at least a proportion of the observed nonstoichiometry. Hence it seems very desirable that samples used for other physical measurements should be examined by electron microscopy, and secondly that the possible influence of intergrowth defects be taken account of in the interpretation of these measurements.

4.3. The Nature of the Defects

An important feature of the idealized models presented here is that in all cases, they indicate that the defects are accommodated in the structures in a coherent way, and are not accompanied by any severe misplacement of neighbouring atoms or groups of atoms. In this respect, they differ entirely from dislocations, observed particularly in metals, where the arrangement of atoms at the core of the defect is heavily distorted, and the associated strain field extends for large distances into the surrounding material. Indeed, it is the presence of this strain field which renders dislocations *visible* in electron micrographs of metal foils, at quite moderate magnifications (say 20,000 ×). The fact that the lattice images presented here (which were recorded at primary magnifications of ca. 200,000 ×) show no deterioration of contrast in the vicinity of the defects indicates that the strain associated with their presence is negligible.

Wadsley intergrowth defects are analogous in some respects to planar defects such as stacking faults in metals, which are not accompanied by extensive strain fields. For example, the defect caused by the presence of two adjacent *D* rows in an otherwise ordered intergrowth of *C* and *D* rows could be regarded as a stacking fault. The presence of a single *D* row in a matrix of *C* rows has the effect of shifting the structure of the matrix on one side of the *D* row by half a unit cell with respect to that on the other side. This situation, which can be seen on the right side of Fig. 2a and also in the vicinity of *D* in Fig. 12b, is analogous to the effect of the presence of an antiphase boundary in an ordered alloy.

4.4. Diffusion of Defects During Annealing

One of the most interesting problems relating to systems exhibiting crystallographic shear concerns the mechanism by which shear planes are formed and how they move. Several models for processes of this kind have been proposed (*17–19*), but there is a general lack of detailed observations with which to compare these models. The most fruitful experimental approach to this problem would be to observe the processes directly in an electron microscope fitted with a high temperature specimen holder. However, the difficulties attending such a study are considerable, principally because of the necessity to obtain images with reasonable resolution, from fragments which are heated to say, 1500 °K. The current approach of examining samples quenched from high temperature is a less satisfactory, but experimentally simpler alternative. The fact that high concentrations of displacement defects, which are not generally found in annealed samples, have been observed indicates that the quenching technique has successfully produced metastable arrangements well removed from the equilibrium conditions which may be attained by annealing. The observations indicate that the abundance of defects of a particular type decreases in the order Wadsley intergrowth > displacements parallel to b > displacements perpendicular to b, and it is tempting to relate this to their relative mobility within the fragments. Another observation which is relevant to this discussion relates to the anisotropy of oxygen diffusion in H–Nb_2O_5. Sheasby and Cox (*20*) found that both in stoichiometric and slightly reduced Nb_2O_5, the diffusion coefficients for oxygen are up to 200 times greater parallel to the b axis than perpendicular to this direction. It might be anticipated therefore that a step on a displacement perpendicular to b (Fig. 7b) might move rapidly in the b direction by diffusion of oxygen (or perhaps metal atoms) in this direction. The motion of such a defect right through a fragment has the effect of shifting a displacement parallel to b by one block in the direction of the shear plane. A continued series of such diffusive motions will finally move the displacement parallel to b right across the crystal, with the result that the shear plane is shifted parallel to b. It is intended to examine this proposal in more detail in a subsequent publication (*12*).

Acknowledgment

I am particularly grateful to Dr. J. V. Sanders for his continued interest in this project, and helpful criticism of the results.

References

1. A. D. WADSLEY, *Rev. Pure Appl. Chem.* **5**, 165 (1955).
2. A. D. WADSLEY, *in* "Non-Stoichiometric Compounds," p. 111 (L. Mandelcorn Ed.), Academic Press, Inc., New York, 1964, p. 111.
3. S. ANDERSSON AND A. D. WADSLEY, *in* "Perspectives in Inorganic Chemistry," Vol. III (J. D. Dunitz and J. A. Ibers, Eds.), John Wiley and Sons, Inc., New York, 1969, in press.
4. J. G. ALLPRESS, J. V. SANDERS, AND A. D. WADSLEY, *Phys. Stat. Sol.* **25**, 541 (1968).
5. J. G. ALLPRESS, J. V. SANDERS, AND A. D. WADSLEY, *Acta Cryst.* **B25**, 1156 (1969).
6. J. G. ALLPRESS AND A. D. WADSLEY, *J. Solid State Chem.* **1**, 28 (1969).
7. J. G. ALLPRESS, *J. Solid State Chem.* **1**, 66 (1969).
8. J. G. ALLPRESS, *Mat. Res. Bull.*, **3**, 1707 (1969).
9. A. D. WADSLEY, *Acta Cryst.* **14**, 664 (1961).
10. S. ANDERSSON, *Z. Anorg. Allgem. Chem.* **351**, 106 (1967).
11. W. MERTIN, S. ANDERSSON, AND R. GRUEHN, *J. Solid State Chem.* (Wadsley Memorial Issue).
12. J. G. ALLPRESS, to be published.
13. G. G. LIBOWITZ, *in* "Progress in Solid State Chemistry," Vol. 2, p. 235. (H. Reiss, Ed.), Pergamon Press, New York, 1965.
14. R. S. ROTH AND A. D. WADSLEY, *Acta Cryst.* **19**, 32 (1965).
15. R. S. ROTH AND A. D. WADSLEY, *Acta Cryst.* **19**, 26 (1965).
16. R. S. ROTH AND J. G. ALLPRESS, unpublished results.
17. P. GADO, *Acta Phys. Acad. Sci. Hung.* **18**, 111 (1965).
18. S. ANDERSSON AND A. D. WADSLEY, *Nature* **211**, 581 (1966).
19. J. S. ANDERSON AND B. G. HYDE, *J. Phys. Chem. Solids* **28**, 1393 (1967).
20. J. S. SHEASBY AND B. COX, *J. Less-Common Metals* **15**, 129 (1968).